Reproducibility of Histogram and Texture Parameters Derived from Intravoxel Incoherent Motion Diffusion-weighted MRI of FN13762 Rat Breast Carcinomas

YONG SUB SONG[1], CHANG MIN PARK[1,2], SANG MIN LEE[1], SANG JOON PARK[1,2], HYE RIM CHO[1], SEUNG HONG CHOI[1], JEONG MIN LEE[1], BERTHOLD KIEFER[3] and JIN MO GOO[1,2]

[1]*Department of Radiology, Seoul National University College of Medicine, and Institute of Radiation Medicine, Seoul National University Medical Research Center, Seoul, Republic of Korea;*
[2]*Cancer Research Institute, Seoul National University, Seoul, Republic of Korea;*
[3]*Siemens Healthcare, Erlangen, Germany*

Abstract. *Aim: To determine the reproducibility of histogram and texture parameters derived from intravoxel incoherent motion (IVIM) diffusion-weighted magnetic resonance imaging (MRI) of FN13762 rat breast carcinomas. Materials and Methods: IVIM diffusion-weighted MRI was performed twice, nine days after tumor implantation in 11 rats. At each session, histogram and texture parameters of entire tumors were extracted from apparent diffusion coefficient (ADC), true-diffusion coefficient (D_t), pseudo-diffusion coefficient (D_p), and perfusion fraction (Pf) maps. Intraobserver and interscan measurement reproducibilities were evaluated using intraclass correlation coefficients (ICC). Results: Mean, entropy, 5th, 10th, 25th percentiles from ADC and D_t maps revealed good intra-observer and interscan agreements [lower limits of 95% confidence interval (CI) for ICC≥0.75]. However, all parameters from Dp and Pf maps gave relatively poor intra-observer and interscan agreements (lower limits of 95% CI for ICC<0.75). Conclusion: Histogram and texture parameters derived from ADC and D_t maps were more reproducible than those from D_p and Pf maps.*

Quantitative analysis of apparent diffusion coefficient (ADC) maps provided by diffusion-weighted magnetic resonance imaging (MRI) has been shown to be a promising tool in the field of oncology in differentiating malignant from benign tumors, monitoring treatment response, detecting residual tumor or recurrence, and in predicting treatment outcome (1-3). ADC measurements can provide valuable information supplementary to conventional anatomic imaging as it reflects the mobility of water molecules within tissue and can sensitively detect increased cellularity, restriction of cellular membrane permeability, as well as disruption of cellular membrane depolarization, which are all common pathological changes observed in malignancies (4, 5). Recently, however, it has been shown that ADC values are affected by capillary perfusion, and thus, intravoxel incoherent motion (IVIM) was proposed to separate 'true-diffusion' from 'pseudo-diffusion' caused by microcirculatory perfusion of blood within capillaries (6). Thereafter, the clinical potential of quantitative analysis of parametric maps derived from IVIM diffusion-weighted MRI has been demonstrated in patients with several diseases including liver cirrhosis, focal hepatic and pancreatic lesions (7-10).

To date, quantitative analysis of ADC and parametric maps derived from IVIM diffusion-weighted MRI has been limited to the measurement of the mean pixel value within a region of interest (ROI) on the maps. Recently, however, more sophisticated analyses, such as histogram or texture analyses, have been applied to these maps and have shown comparable or superior performance as imaging biomarkers in the evaluation of the fibrosis stage and inflammatory activity of chronic hepatitis, differentiation of glioma grade, and in monitoring treatment response in glioblastoma patients (11-13). Further studies validating variable histogram or texture parameters may uncover additional biomarkers that can provide even more information through non-invasive assessment of target lesions, however, prior to its clinical application, reproducibility of the measurements of eligible imaging biomarkers should first be examined (14).

Correspondence to: Chang Min Park, MD, Department of Radiology, Seoul National University Hospital, 101, Daehangno, Jongno-gu, Seoul 110-744, Korea. Tel: +82 220720367, Fax: +82 27437418, e-mail: cmpark@radiol.snu.ac.kr

Key Words: Reproducibility, histogram, texture, intravoxel incoherent motion, diffusion-weighted MRI, FN13762 rat breast carcinoma.

To our knowledge, however, there have been few studies on the reproducibility of measurements of histogram and texture parameters derived from ADC maps (11, 15), and nor of those parameters derived from IVIM MRI. Thus, the purpose of our study was to determine the reproducibility of histogram and texture parameters derived from IVIM diffusion-weighted MRI of FN13762 rat breast carcinomas.

Materials and Methods

This study was approved by the Animal Care and Use Committee of our Hospital [#13-0322-C0A0 (1)].

Tumor cell line, experimental animals and tumor implantation. The FN13762 murine mammary carcinoma cell line (American Type Culture Collection, Manassas, VA, USA) was used as the experimental animal tumor model in our study. FN13762 carcinoma has been shown to be a spontaneously metastatic syngeneic rat tumor, which has been extensively characterized for both its in vitro and in vivo growth (16).

Eleven female Fischer 344 rats (weight range, 250-300 g; Charles River, Sulzbach, Germany) were anesthetized for tumor cell implantation by injecting a solution of zolazepam (5 mg/kg, Zoletil®; Virbac, Carros, France) and xylazine (10 mg/kg, Rompun®; Bayer-Schering Pharma, Berlin, Germany) into their hindlimbs. After anesthesia, FN13762 cells were inoculated into the muscular layer of the right upper thigh of the rats with a 24-guage needle by injecting 4×10^5 cells suspended in 0.1 ml of Dulbecco's modified Eagle's medium (Cambrex Biosciences, Verviers, France). Cellular viability was tested prior to tumor implantation using trypan blue, which yielded a result greater than 90%. All procedures were performed using the aseptic technique.

MRI acquisition. After a 9-day feeding period, MRI scans were performed with a 3-T MRI system with a 6-channel rat body coil (Stark Contrast, Erlangen, Germany). Firstly, we acquired axial T2-weighted turbo spin-echo images (TR/TE, 8930/101 ms; bandwidth, 196 Hz/pixel; flip angle, 120°; field of view, 100×81 mm; matrix, 192×115; slice thickness, 0.8 mm; number of signals, 8) of the lower-half of the rat's body under anesthesia using zolazepam and xylazine. Thereafter, for IVIM diffusion-weighted MRI, one radiologist (YSS with three years of experience in body MRI) reviewed the T2-weighted images and determined the scan range to cover the entire volume of the tumor. IVIM diffusion-weighted MRIs were performed using single-shot echo-planar prototype imaging pulse sequence (Siemens Healthcare, Erlangen, Germany) with diffusion gradients applied in three orthogonal directions, data acquisition in free breathing, with the following parameters: TR/TE, 4400/73 ms; bandwidth, 798 Hz/pixel; field of view, 100×100 mm; matrix, 128×128; section thickness, 3 mm; number of signals, 8; and multiple b-values, 0, 25, 50, 75, 100, 200, 400, 800 and 1000 s/mm^2. To shorten the echo train length, the parallel imaging technique (generalized autocalibrating partially parallel acquisitions; GRAPPA) with a two-fold acceleration factor was used. To assess the interscan reproducibility of the parameters derived from IVIM diffusion-weighted MRI, all rats underwent IVIM diffusion-weighted MRI twice, with the examinations set 5 minutes apart.

IVIM parametric map acquisition. Diffusion-weighted MRI data were post-processed using prototype software (Siemens Healthcare) to extract ADC and IVIM parameters composed of the true-diffusion coefficient (D_t), representing pure molecular diffusibility; pseudo-diffusion coefficient (D_p), representing perfusion-related incoherent microcirculation; and perfusion fraction (*Pf*), which has been linked to blood volume (17). ADC values were automatically calculated using all b values with a monoexponential fit using the following equation: $SI/SI_0=\exp(-b\times ADC)$, where SI_0 is the mean signal intensity of the ROI for the b value of 0 sec/mm^2 and SI is the signal intensity for the higher b values. On the basis of the IVIM concept, D_t, D_p and *Pf* values were calculated using a nonlinear biexponential fit according to the following equation (18): $SI/SI_0=(1 - Pf)\cdot\exp(-b\cdot D_t) + Pf\cdot\exp(-b\cdot D_p)$. Four parametric maps of ADC, D_t, D_p and *Pf* were created on a pixel-by-pixel basis for each animal (Figure 1).

Image analysis. One radiologist (SML with eight years of experience in body MRI) manually drew the ROI to encompass as much of the whole tumor as possible on all ADC maps from the first IVIM MRI using in-house software (Figure 2). Care was taken to avoid non-tumor tissues on the ADC maps. To evaluate intra-observer measurement reproducibility, the observer drew ROIs of whole tumors again on the ADC maps obtained from the first IVIM MRI four weeks later. As for interscan measurement reproducibility, the observer separately segmented the same tumors on ADC maps obtained from the first IVIM MRIs and those from the second IVIM MRIs. These segmentations were conducted separately with at least a 4-week interval. ROIs were then copied from the ADC map and placed on the other corresponding parametric maps for D_t, D_p and *Pf*. After the ROIs were placed, ROI volume, histogram and texture parameters were calculated and automatically extracted. Histogram parameters included: (a) mean, (b) standard deviation (SD), (c) skewness, (d) kurtosis and (e) percentile values (5th, 10th, 25th, 50th, 75th and 90th). Texture parameters included: (a) entropy, (b) homogeneity, (c) gray-level co-occurrence matrix (GLCM) inverse difference moment (IDM) and (d) GLCM contrast.

Calculation of histogram and texture parameters. Skewness represents the distribution pattern of the degree of pixel values on histograms. Negative and positive skewness indicates that the pixel values are more spread to the left and right of the mean, respectively (19). Kurtosis represents the position of the peak height, which indicates the pixel value of the maximum frequency on histograms. A normal distribution has a kurtosis of 0, a leptokurtic one is indicated by a sharper peak and has a kurtosis of more than 0, and a platykurtic distribution is indicated by a flatter peak with a kurtosis of less than 0 (19). Parameters are defined mathematically below, where N is the number of data points in a region-of-interest, $\bar{x}$ is the mean and s is the standard deviation.

$$\text{Skewness} = \frac{1}{(N-1)s^3}\sum_{i=1}^{N}\left(X_i-\bar{X}\right)^3$$

$$\text{Kurtosis} = \frac{1}{(N-1)s^4}\sum_{i=1}^{N}\left(X_i-\bar{X}\right)^4$$

Heterogeneity within the tumor was assessed with entropy and homogeneity. Entropy is a parameter reflecting the unpredictability of any information content of an image and has been widely used

in information theory (20). Homogeneity is the measure that increases with less contrast in the window, and was calculated using a two-dimensional image histogram for the purposes of this study (21). High entropy and low homogeneity values indicate increased heterogeneity of the tumor. Parameters are defined mathematically below, where G is the number of gray levels in a ROI and $P(I)$ is the probability of the occurrence of a gray level I on a histogram.

$$\text{Entropy} = -\sum_{i=1} [P(I)] \log_2 [P(I)]$$

$$\text{Homogeneity} = \sum_{i=1}^{G-1} \sum_{j=1}^{G-1} \frac{1}{1+(I-J)} P(I,J)$$

GLCM is a matrix where element $P(I, J)$ is relative frequency with which a combination of two pixels with intensity I and J occur in an image, separated by a given distance. A number of texture features may be extracted from the GLCM and two texture features calculated from the GLCM were used in this study. A GLCM inverse difference moment (IDM) is influenced by the homogeneity of the image and GLCM contrast reflects the local intensity variation (22).

$$\text{GLCM IDM} = \sum_{i=0}^{G-1} \sum_{j=0}^{G-1} \frac{1}{1+(i-j)^2} P(i,j)$$

$$\text{GLCM contrast} = \sum_{n=0}^{G-1} n^2 \left\{ \sum_{i=1}^{G} \sum_{j=1}^{G} P(i,j) \right\}, \qquad |i-j| = n$$

Statistical analysis. We compared all parameters between the first and second measurements on the first IVIM MRI for the intra-observer reproducibility test, and between the first measurements on the first IVIM MRI and the second IVIM MRI for the interscan reproducibility test.

The paired *t*-test was used to assess the presence of any systemic bias in intra-observer and interscan comparisons for all parameters. Results with *p*-values of less than 0.05 were considered to indicate a statistically significant difference. Reproducibilities of all parameters were then evaluated using intraclass correlation coefficients (ICC). The lower limit of the 95% confidence interval (CI) for ICC ≥0.75 was considered to represent good agreement (23). We designated each parameter as a reproducible parameter when all the following conditions were satisfied in both intra-observer and interscan comparisons: (a) no systemic bias according to the paired *t*-test and (b) good agreement according to the ICC. To estimate the magnitude of measurement variability in all parameters, 95% limits of agreement in intraobserver and interscan comparisons were obtained according to the Bland-Altman method. Results of the Bland-Altman method were expressed as absolute values for skewness, kurtosis, entropy, homogeneity, GLCM IDM and GLCM contrast, and were transformed as percentages for mean, SD and percentile values as variabilities of those parameters were not independent of the magnitude of the measurement.

All statistical analyses were performed using Medcalc (version 12.7.2.0, MedCalc Software, Mariakerke, Belgium).

Results

The mean diameter of all 11 tumors was 14.36±3.00 mm (range=10.63-19.72 mm). As for volume measurements, there were no significant mean differences in terms of intra-observer variability nor interscan variability ($p>0.05$). Their ICCs were 0.99 (95% CI=0.97-1.00) and 0.99 (95% CI=0.95-1.00) for intra-observer and interscan comparisons, respectively. The 95% limits of agreement in intra-observer and interscan comparisons ranged from −18.2% to 18.0% (mean=−0.1%) and −27.5% to 25.7% (mean, −0.9%) of the ROI volumes, respectively.

ADC map. There were no significant differences in the mean values, SD, skewness, kurtosis, all percentile values (5th, 10th, 25th, 50th, 75th and 90th), entropy, homogeneity, GLCM IDM and GLCM contrast of ADC values from ADC maps in terms of both intra-observer and interscan comparisons ($p>0.05$). Table I summarizes the results of ICCs and Bland-Altman methods in intra-observer and interscan comparisons for all parameters from the ADC maps. For intra-observer comparison, mean, entropy, GLCM contrast and all percentile values showed good agreement, with lower limits of 95% CI for ICC ranging from 0.85 to 1.00. For interscan comparison, mean, entropy, 5th, 10th, 25th and 90th percentile values showed good agreement, with lower limits of 95% CI for ICC ranging from 0.77 to 0.94.

D_t map. There was a significance difference in kurtosis in terms of interscan comparison ($p=0.034$). Table II summarizes the results of ICCs and Bland-Altman methods in intraobserver and interscan comparisons for all parameters from the Dt maps. For intra-observer comparison, mean, entropy, GLCM contrast and all percentile values showed good agreement, with lower limits of 95% CI for ICC ranging from 0.87 to 1.00. For interscan comparison, mean, entropy, GLCM contrast, 5th, 10th, 25th and 50th percentile values showed good agreement, with lower limits of 95% CI for ICC ranging from 0.77 to 0.96.

D_p map. There were no significant differences in the mean values, SD, skewness, kurtosis, all percentile values (5th, 10th, 25th, 50th, 75th and 90th), entropy, homogeneity, GLCM IDM and GLCM contrast of D_p values from D_p maps in terms of both intra-observer and interscan comparisons ($p>0.05$). Table III summarizes the results of ICCs and Bland-Altman methods in intra-observer and interscan comparisons for all parameters from the D_p maps. For intra-observer comparison, mean, kurtosis, entropy, homogeneity, GLCM IDM, 25th, 50th and 75th percentile values showed

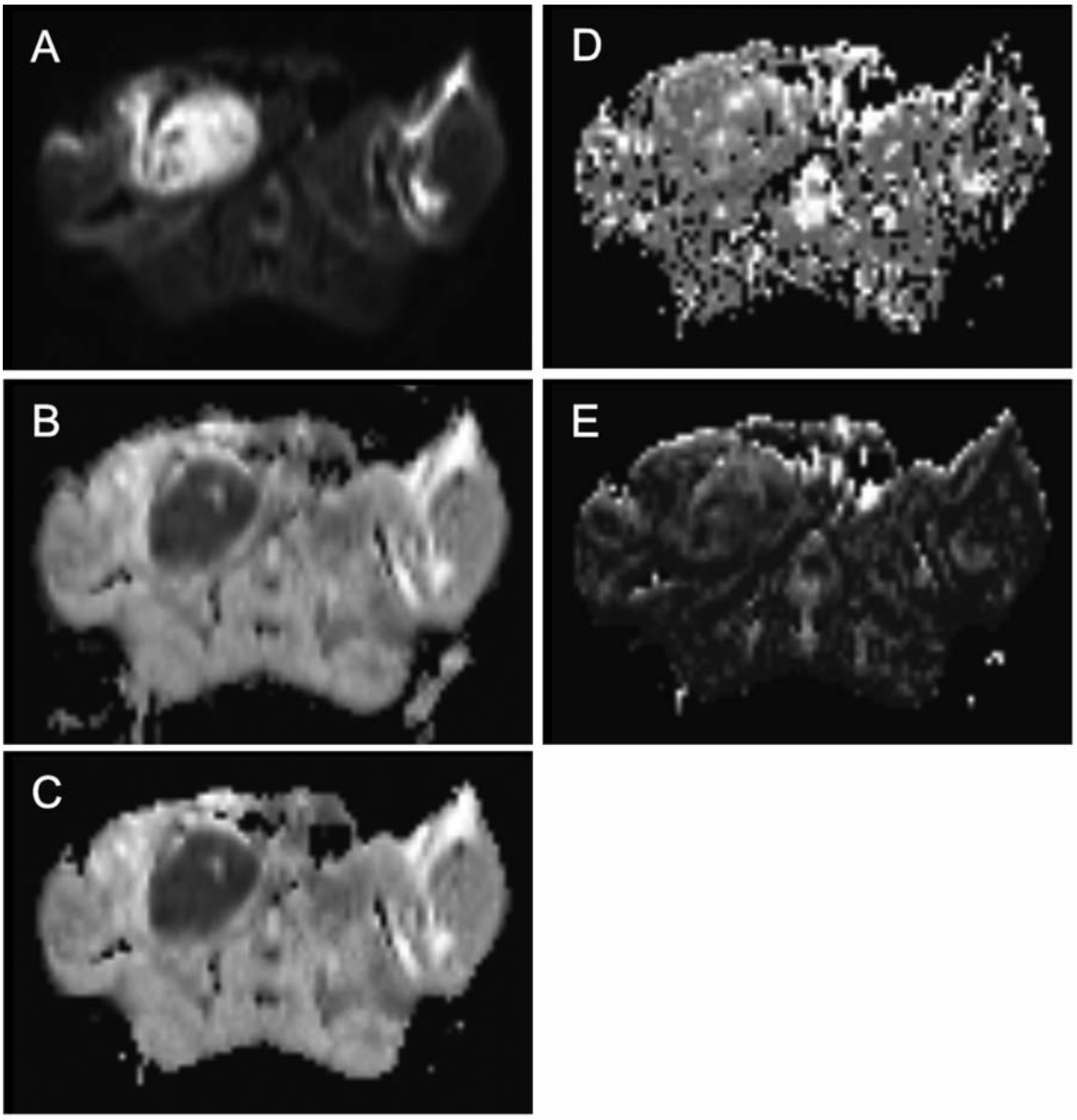

Figure 1. *An FN13762 rat breast cancer in a rat model. Axial diffusion-weighted image of the tumor in the right hindlimb (b=200 s/mm^2) (A) and corresponding apparent diffusion coefficient map (B). Intravoxel incoherent motion diffusion-weighted magnetic resonance imaging parametric maps of true-diffusion coefficient, pseudo-diffusion coefficient and perfusion fraction are demonstrated in C-E, respectively.*

good agreement, with lower limits of 95% CI for ICC ranging from 0.77 to 0.99. For interscan comparison, however, no parameter showed good agreement.

Pf map. There was a significant difference in the Pf values in terms of intra-observer comparison (p=0.049). Table IV summarizes the results of ICCs and Bland-Altman methods in intraobserver and interscan comparisons for all parameters from *Pf* maps. For intra-observer comparison, mean, 10th, 25th, 50th, 75th and 90th percentile values showed good agreement, with lower limits of 95% CI for ICC ranging from 0.87 to 1.00. For interscan comparison, however, no parameter showed good agreement.

Discussion

In our study, we evaluated the reproducibility of various parameters of ADC maps and parametric maps derived from

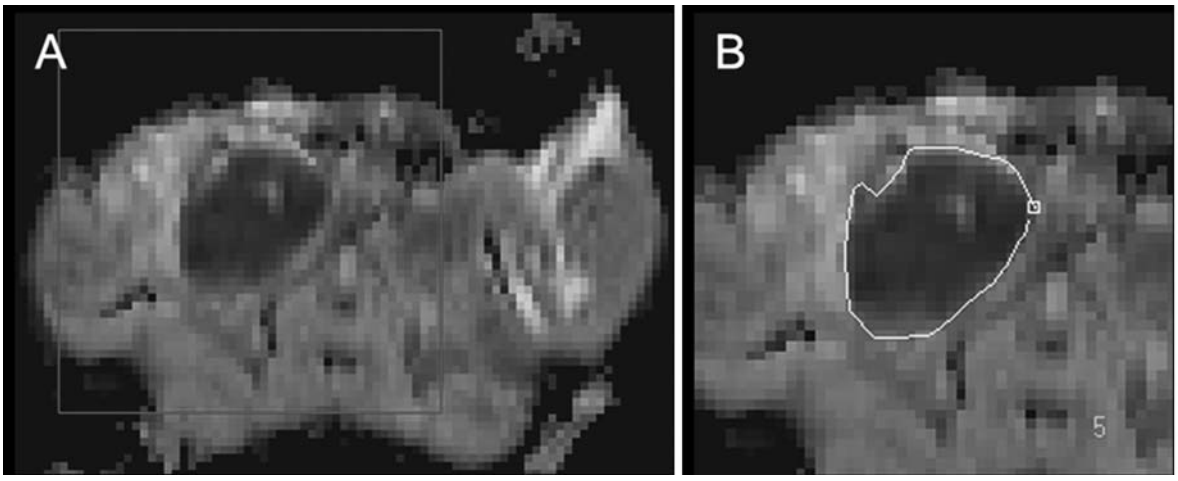

Figure 2. *In-house software program for histogram and texture parameter measurements. This software program provides two screens of loaded images with or without magnification. A: Loaded apparent diffusion coefficient map without magnification. The marked area was selected for magnification. B: 1.3-Fold magnified image of the area shown in A. The region of interest (shown as polymorphic lines; the square on the line indicates the starting point for drawing the region-of-interest) was performed on this magnified image. The number on the image indicates the current image number of the ADC map stack.*

IVIM diffusion-weighted MRI in terms of both intraobserver and interscan variabilities. Diffusion-weighted MRI was repeated in a single imaging session in a very short time interval, so that changes in the tumor microenvironment or in the physiological status of the animals would have been negligible, reflecting the measurement error that can result from image noise, image distortion and motion artifacts, as well as intra-observer variability in drawing an ROI. Indeed, all parameters that failed to attain good intra-observer agreement in our study also failed to attain good interscan agreements. Acceptable interscan reproducibility is essential for any imaging biomarker, as at least two sets of images scanned at different time points are required to evaluate changes in the imaging biomarker. Our study showed that several histogram and texture parameters can be reproducibly-measured from ADC and D_t maps of FN13762 rat breast carcinomas. Those parameters were the mean, entropy, 5th, 10th, 25th and 90th percentile values from ADC maps, and mean, entropy, GLCM contrast, 5th, 10th, 25th and 50th percentile values from D_t maps.

The mean ADC and D_t values have been widely used as representative values of a target lesion in oncological imaging (24), and their good reproducibility has been reported in both animal and human studies (11, 17, 25). Another fact that may have positively influenced the reproducibility of the mean value in our study was the method of ROI drawing employed, namely that we calculated the mean value by averaging all pixel values from whole-tumor volumes. Indeed, Lambregts *et al*. reported that ADC measurements obtained from whole-tumor volumes are more reproducible than those obtained from single-slice or small sample ROIs (26). A previous clinical trial also reported the good reproducibility of ADC and perfusion-insensitive ADC values from ROIs encasing whole-tumor volumes (27).

Entropy describes the variation in a volume histogram of pixel values and has been shown to be a promising indicator of tumor heterogeneity (28). In addition, SD, homogeneity, GLCM IDM and GLCM contrast values also measure a particular characteristic of the distribution between pixels in the ROI (29), and can thus reflect tumor heterogeneity. However, as those variables are inter-dependent, the selection of fewer parameters, with the advantage of measurement reproducibility, may be a more practical approach in discovering new imaging biomarkers. According to our results, the entropy from both ADC and D_t maps, and GLCM contrast from the D_t map showed better reproducibility than other parameters. Fujimoto *et al*. also observed good interobserver reproducibility of entropy from ADC maps of the liver parenchyma in patients with chronic hepatitis C and reported that the coefficient of repeatability (*i.e*. 1.96-times the SD of the difference between the two measurements) was 0.072 (11). In our entropy measurement from FN13762 rat breast carcinomas, coefficients of repeatability were 0.096 and 0.118 for intraobserver and interscan comparisons, respectively. Jensen *et al*. also showed good interscan reproducibility of ADC entropy, for which the ICC was 0.84 (CI was not presented there) in patients with breast cancer (25).

Lower percentile values (*i.e*., 5th, 10th and 25th percentile values) of ADC and D_t histograms were chosen to account for tumor heterogeneity in our study and are regarded as a promising measurement method, which may sensitively detect

Table I. *Results of intraclass correlation coefficients (ICC) and the Bland–Altman method for all parameters from apparent diffusion coefficient maps.*

	Intraobserver reproducibility test				Interscan reproducibility test			
			Bland–Altman method				Bland–Altman method	
	ICC	95% CI	95% LOA	Mean	ICC	95% CI	95% LOA	Mean
Mean	0.98	0.92-0.99	–8.28%-8.13%	–0.08%	0.93	0.77-0.98	–12.15%-11.50%	–0.33%
SD	0.92	0.72-0.98	–22.33%-24.30%	0.98%	0.91	0.72-0.98	–20.59%-20.82%	0.11%
Skewness†	0.89	0.64-0.97	–0.304-0.406	0.051	0.86	0.56-0.96	–0.255-0.504	0.125
Kurtosis†	0.91	0.69-0.97	–0.882-1.187	0.153	0.91	0.72-0.98	–0.630-1.227	0.299
Entropy†	0.98	0.91-0.99	–0.175-0.187	0.006	0.96	0.86-0.99	–0.249-0.213	–0.018
Homogeneity†	0.90	0.66-0.97	–0.004-0.005	0.000	–0.12	–0.65-0.49	–0.019-0.017	–0.001
GLCM IDM†	0.92	0.72-0.98	–0.004-0.003	0.000	–0.20	–0.69-0.43	–0.017-0.014	–0.002
GLCM Contrast†	0.98	0.92-0.99	–2.664-2.470	–0.097	0.92	0.72-0.98	–6.078-5.188	–0.445
5th percentile	1.00	0.99-1.00	–3.29%-3.65%	0.18%	0.97	0.90-0.99	–6.84%-11.59%	2.38%
10th percentile	1.00	1.00-1.00	–1.68%-2.51%	0.42%	0.98	0.94-1.00	–5.68%-9.38%	1.85%
25th percentile	0.99	0.98-1.00	–5.30%-5.45%	0.07%	0.97	0.90-0.99	–10.40%-10.38%	–0.01%
50th percentile	0.96	0.86-0.99	–11.88%-10.71%	–0.59%	0.92	0.74-0.98	–16.67%-12.78%	–1.95%
75th percentile	0.97	0.91-0.99	–7.91%-7.91%	0.00%	0.89	0.63-0.97	–16.00%-12.60%	–1.70%
90th percentile	0.96	0.85-0.99	–12.75%-12.51%	–0.12%	0.94	0.79-0.98	–13.78%-13.78%	0.00%

CI: Confidence interval, LOA: limit of agreement, SD: standard deviation, GLCM: gray–level co–occurrence matrix and IDM: inverse difference moment. †Expressed as an absolute value in the Bland–Altman method.

Table II. *Results of intraclass correlation coefficients (ICC) and the Bland–Altman method for all parameters from true-diffusion coefficient maps.*

	Intraobserver reproducibility test				Interscan reproducibility test			
			Bland–Altman method				Bland–Altman method	
	ICC	95% CI	95% LOA	Mean	ICC	95% CI	95% LOA	Mean
Mean	0.98	0.92-0.99	–8.84%-8.47%	–0.19%	0.95	0.81-0.99	–11.51%-10.70%	–0.40%
SD	0.91	0.70-0.97	–24.25%-26.46%	1.11%	0.90	0.68-0.97	–22.99%-21.93%	–0.53%
Skewness†	0.91	0.70-0.97	–0.318-0.390	0.036	0.87	0.58-0.96	–0.290-0.516	0.113
Kurtosis†	0.89	0.66-0.97	–1.054-1.424	0.185	0.92	0.73-0.98	–0.646-1.429	0.391
Entropy†	0.97	0.89-0.99	–0.191-0.187	–0.002	0.97	0.90-0.99	–0.199-0.169	–0.015
Homogeneity†	0.90	0.66-0.97	–0.003-0.002	–0.001	–0.36	–0.77-0.27	–0.016-0.013	–0.002
GLCM IDM†	0.83	0.48-0.95	–0.003-0.002	0.000	–0.48	–0.83-0.13	–0.016-0.011	–0.002
GLCM Contrast†	0.98	0.92-0.99	–2.746-2.465	–0.141	0.93	0.77-0.98	–5.535-4.612	–0.462
5th percentile	1.00	0.99-1.00	–3.02%-3.33%	0.15%	0.97	0.89-0.99	–5.17%-11.30%	3.06%
10th percentile	1.00	1.00-1.00	–1.54%-1.89%	0.18%	0.99	0.96-1.00	–4.21%-8.43%	2.11%
25th percentile	1.00	0.98-1.00	–5.48%-4.33%	–0.58%	0.98	0.92-0.99	–8.03%-9.60%	0.78%
50th percentile	0.96	0.87-0.99	–12.45%-10.60%	–0.92%	0.95	0.84-0.99	–13.66%-10.33%	–1.67%
75th percentile	0.98	0.93-0.99	–8.42%-7.19%	–0.62%	0.91	0.72-0.98	–15.56%-10.69%	–2.44%
90th percentile	0.97	0.88-0.99	–11.67%-12.05%	0.19%	0.92	0.73-0.98	–16.57%-15.07%	–0.75%

CI: Confidence interval, LOA: limit of agreement, SD: standard deviation, GLCM: gray–level co–occurrence matrix and IDM: inverse difference moment. †Expressed as an absolute value in the Bland–Altman method.

focal regions of higher cellularity (12, 13, 30, 31). Our results showed that those parameters can be consistently measured in both ADC and D_t histograms of small animal tumors. The 50th percentile value, as well as the 10th and 25th percentile values, of ADC histograms was also suggested as a useful parameter in the prediction of the low-grade glioma subtype (32), but showed relatively worse reproducibility than the lower percentile values (*i.e.* 5th, 10th and 25th percentile values) in our study. On the other hand, the 50th percentile value of D_t histograms showed slightly better reproducibility

Table III. *Results of intraclass correlation coefficients (ICC) and the Bland–Altman method for all parameters from pseudo-diffusion coefficient maps.*

	Intraobserver reproducibility test				Interscan reproducibility test			
			Bland–Altman method				Bland–Altman method	
	ICC	95% CI	95% LOA	Mean	ICC	95% CI	95% LOA	Mean
Mean	0.93	0.77-0.98	–3.90-5.12%	0.61%	0.59	0.03-0.87	–15.92-10.05%	–2.93%
SD	0.44	–0.18-0.81	–35.58-47.93%	6.17%	0.60	0.04-0.87	–40.79-29.69%	–5.55%
Skewness†	0.90	0.67-0.97	–0.790-0.974	0.092	0.50	–0.10-0.84	–2.319-1.798	–0.261
Kurtosis†	0.96	0.87-0.99	–2.320-1.852	–0.234	0.34	–0.29-0.77	–9.109-8.855	–0.127
Entropy†	0.96	0.86-0.99	–0.163-0.215	0.026	0.54	–0.06-0.85	–0.650-0.509	–0.071
Homogeneity†	0.97	0.91-0.99	–0.005-0.005	0.000	0.75	0.31-0.93	–0.013-0.017	0.002
GLCM IDM†	0.93	0.77-0.98	–0.004-0.003	0.000	0.32	–0.32-0.76	–0.015-0.015	0.000
GLCM Contrast†	0.90	0.67-0.97	–0.331-0.439	0.054	0.60	0.04-0.88	–1.219-0.768	–0.226
5th percentile	0.56	–0.03-0.86	–308.49-361.05%	26.28%	0.09	–0.52-0.63	–435.73-486.33%	25.30%
10th percentile	0.87	0.58-0.96	–179.89-132.81%	–23.54%	0.25	–0.39-0.72	–496.00-544.33%	24.17%
25th percentile	1.00	0.99-1.00	–1.94-2.34%	0.20%	–0.23	–0.71-0.40	–47.98-36.57%	–5.70%
50th percentile	0.98	0.91-0.99	–2.36-1.96%	–0.20%	0.56	–0.03-0.86	–11.90-9.55%	–1.18%
75th percentile	0.94	0.79-0.98	–3.79-4.85%	0.53%	0.70	0.21-0.91	–15.29-8.74%	–3.27%
90th percentile	0.80	0.42-0.94	–9.13-10.18%	0.52%	0.59	0.02-0.87	–22.94-12.25%	–5.34%

CI: Confidence interval, LOA: limit of agreement, SD: standard deviation, GLCM: gray–level co–occurrence matrix and IDM: inverse difference moment. †Expressed as an absolute value in the Bland–Altman method.

Table IV. *Results of intraclass correlation coefficients (ICC) and the Bland–Altman method for all parameters from perfusion fraction maps*

	Intraobserver reproducibility test				Interscan reproducibility test			
			Bland–Altman method				Bland–Altman method	
	ICC	95% CI	95% LOA	Mean	ICC	95% CI	95% LOA	Mean
Mean	0.98	0.91-0.99	–3.20%-6.56%	1.68%	0.27	–0.36-0.73	–34.94%-30.29%	–2.33%
SD	0.79	0.38-0.94	–49.63%-75.37%	12.87%	0.50	–0.10-0.84	–71.02%-87.98%	8.48%
Skewness†	0.32	–0.31-0.76	–1.110-1.247	0.069	0.20	–0.42-0.70	–2.107-1.789	–0.159
Kurtosis†	0.33	–0.31-0.76	–6.841-6.301	–0.270	0.15	–0.47-0.67	–20.100-14.861	–2.620
Entropy†	–0.04	–0.60-0.55	–1.560-2.124	0.282	–0.06	–0.61-0.54	–1.662-2.177	0.258
Homogeneity†	0.52	–0.08-0.84	–0.006-0.009	0.002	0.37	–0.26-0.78	–0.007-0.011	0.002
GLCM IDM†	0.29	–0.34-0.74	–0.001-0.002	0.001	–0.09	–0.63-0.51	–0.003-0.004	0.000
GLCM Contrast†	0.02	–0.57-0.59	–4.000-5.528	0.764	0.01	–0.57-0.58	–4.165-5.533	0.684
5th percentile	0.61	0.05-0.88	–191.46%-192.95%	0.74%	0.07	–0.53-0.62	–282.50%-321.43%	19.46%
10th percentile	1.00	1.00-1.00	–7.44%-10.34%	1.45%	–0.09	–0.63-0.51	–198.02%-191.12%	–3.45%
25th percentile	0.96	0.87-0.99	–11.17%-10.14%	–0.52%	0.24	–0.39-0.72	–62.85%-48.49%	–7.18%
50th percentile	0.97	0.89-0.99	–5.71%-6.69%	0.49%	0.18	–0.44-0.68	–38.63%-31.85%	–3.39%
75th percentile	0.98	0.95-1.00	–3.92%-6.51%	1.29%	0.56	–0.03-0.86	–30.42%-25.42%	–2.50%
90th percentile	0.99	0.96-1.00	–3.75%-6.36%	1.30%	0.57	–0.01-0.86	–32.29%-31.30%	–0.49%

CI: Confidence interval, LOA: limit of agreement, SD: standard deviation, GLCM: gray–level co–occurrence matrix and IDM: inverse difference moment. †Expressed as an absolute value in the Bland–Altman method.

than that of ADC histograms. In addition, the 90th percentile value of ADC and D_t histograms has been shown to reflect low cellularity regions within the tumor such as necrosis or cystic change (24, 33), and was slightly more reproducible in ADC histograms than D_t histograms in our study.

We also found that kurtosis and skewness measurements from ADC histograms exhibited relatively worse reproducibility in FN13762 rat breast carcinomas. Those parameters from ADC maps had previously been suggested as potential imaging biomarkers for prediction of chemotherapy

response and progression-free survival in various malignancies (25, 31). However, according to Jensen *et al*. (25) who investigated the interscan reliability of ADC mean, skewness, and entropy in patients with breast cancer, the interscan ICC of ADC skewness (0.75; 95% CI was not presented there) was shown to be relatively worse than that of ADC mean and entropy (0.84), which is compatible with our results.

All parameters in D_p and *Pf* maps in our study had relatively worse reproducibility than ADC or D_t maps. Some parameters showed good intraobserver agreement, whereas all parameters failed to attain good interscan agreement on ICC analyses. Both perfusion-sensitive parameters were calculated from biexponential fitting of IVIM diffusion-weighted MRI data at multiple lower b values. However, signal measurements at low b-values, especially those ≤100 s/mm^2, are known to be more prone to measurement errors and highly sensitive to signal-to-noise variations, thus hindering consistent model fitting (33). Andreou *et al*. also reported the poor measurement reproducibility of mean D_p and *Pf* in liver metastases, with a very wide 95% CI of differences (−89% to 2,120% and −75.3% to 241% for D_p and *Pf*, respectively) (34), and Koh *et al*. demonstrated the poor measurement reproducibility of ADC values calculated using low b values (27). They also found a large SD in the estimation of *Pf* (35). In this context, they described that voxel-by-voxel analysis may be inappropriate for perfusion-sensitive parameters (33), which is also supported by our results. In spite of the poor reproducibility, however, several studies reported significant differences in perfusion-sensitive parameters according to the target lesions (35-37). In colorectal liver metastases, the estimated *Pf* was significantly lower than that in normal liver parenchyma (35), in keeping with the hypovascular nature of these lesions. Shinmoto *et al*. reported that both fast (pseudo-diffusion) and slow (true-diffusion) ADCs were lower in prostate cancer than normal peripheral or transitional zones (36), and Lemke *et al*. demonstrated that the Pf of pancreatic carcinoma was significantly lower than normal pancreatic parenchyma (37). However, at present, there is no standard vendor software for biexponential model fitting of IVIM diffusion-weighted MRI data and there is no consensus or an established IVIM diffusion-weighted MRI protocol such as the number and choice of b-values or the number of signal averages. Thus, as previous studies (7-10, 35-37) on IVIM have used variable software and imaging protocols with a variable number of b-values, our results do not indicate inferiority of perfusion-sensitive parameters from any kind of IVIM technique and do not contradict the previously reported usefulness of those parameters (35-37). Further studies optimizing and individualizing the IVIM technique may improve the aforementioned errors in the measurement of perfusion-sensitive parameters. Furthermore, although the error of measurement of a certain parameter may be substantial, the parameter may still be used as an imaging biomarker when the change of scale of the parameter under certain clinical situations exceeds the measurement error. Therefore, histogram and texture parameters from perfusion-sensitive parametric maps still have potential clinical application, despite their relatively poor reproducibility.

Our study has several limitations. Firstly, there were a relatively small number of subjects in the evaluation of measurement reproducibility of the parameters from ADC and parametric maps derived from IVIM MRI. Second by, all MRI scans for tumors were performed at the same time point of tumor growth, which might have caused relatively uniform pathological states of the tumors. This may also have led to overestimation of intraobserver and interscan reproducibilities of the parameters. Finally, all parameters were measured by one observer, and hence measurements may be significantly influenced by the observer.

In conclusion, histogram and texture parameters derived from ADC and Dt maps were more reproducible than those from D_p and *Pf* maps. In addition, mean, entropy, 5th, 10th, 25th percentile values from ADC and D_t maps were reproducible.

Acknowledgements

This research was supported by the Basic Science Research Program through the National Research Foundation of Korea (NRF) funded by the Ministry of Education, Science and Technology (grant number: 2011-0022379).

References

1 Taouli B, Vilgrain V, Dumont E, Daire JL, Fan B and Menu Y: Evaluation of liver diffusion isotropy and characterization of focal hepatic lesions with two single-shot echo-planar MR imaging sequences: prospective study in 66 patients. Radiology *226(1)*: 71-78, 2003.

2 Thoeny HC, De Keyzer F, Chen F, Ni Y, Landuyt W, Verbeken EK, Bosmans H, Marchal G and Hermans R: Diffusion-weighted MR imaging in monitoring the effect of a vascular targeting agent on rhabdomyosarcoma in rats. Radiology *234(3)*: 756-764, 2005.

3 Pickles MD, Gibbs P, Lowry M and Turnbull LW: Diffusion changes precede size reduction in neoadjuvant treatment of breast cancer. Magn Reson Imaging *24(7)*: 843-847, 2006.

4 Kamel IR, Bluemke DA, Ramsey D, Abusedera M, Torbenson M, Eng J, Szarf G and Geschwind JF: Role of diffusion-weighted imaging in estimating tumor necrosis after chemoembolization of hepatocellular carcinoma. Am J Roentgenol *181(3)*: 708-710, 2003.

5 Malayeri AA, El Khouli RH, Zaheer A, Jacobs MA, Corona-Villalobos CP, Kamel IR and Macura KJ: Principles and applications of diffusion-weighted imaging in cancer detection, staging and treatment follow-up. Radiographics *31(6)*: 1773-1791, 2011.

6 Le Bihan D, Breton E, Lallemand D, Aubin ML, Vignaud J and Laval-Jeantet M: Separation of diffusion and perfusion in intravoxel incoherent motion MR imaging. Radiology *168(2)*: 497-505, 1988.

7 Yoon JH, Lee JM, Yu MH, Kiefer B, Han JK and Choi BI: Evaluation of hepatic focal lesions using diffusion-weighted MR imaging: Comparison of apparent diffusion coefficient and intravoxel incoherent motion-derived parameters. J Magn Reson Imaging *39(2)*: 276-285, 2014.

8 Sumi M, Van Cauteren M, Sumi T, Obara M, Ichikawa Y and Nakamura T: Salivary gland tumors: Use of intravoxel incoherent motion MR imaging for assessment of diffusion and perfusion for the differentiation of benign from malignant tumors. Radiology *263(3)*: 770-777, 2012.

9 Luciani A, Vignaud A, Cavet M, Nhieu JT, Mallat A, Ruel L, Laurent A, Deux JF, Brugieres P and Rahmouni A: Liver cirrhosis: Intravoxel incoherent motion MR imaging–pilot study. Radiology *249(3)*: 891-899, 2008.

10 Kang KM, Lee JM, Yoon JH, Kiefer B, Han JK and Choi BI: Intravoxel incoherent motion diffusion-weighted MR imaging for characterization of focal pancreatic lesions. Radiology *270(2)*: 444-453, 2014.

11 Fujimoto K, Tonan T, Azuma S, Kage M, Nakashima O, Johkoh T, Hayabuchi N, Okuda K, Kawaguchi T, Sata M and Qayyum A: Evaluation of the mean and entropy of apparent diffusion coefficient values in chronic hepatitis C: Correlation with pathologic fibrosis stage and inflammatory activity grade. Radiology *258(3)*: 739-748, 2011.

12 Kim HS, Suh CH, Kim N, Choi CG and Kim SJ: Histogram analysis of intravoxel incoherent motion for differentiating recurrent tumor from treatment effect in patients with glioblastoma: Initial clinical experience. Am J Neuroradiol 2013 Aug 22 [Epub ahead of print].

13 Song YS, Choi SH, Park CK, Yi KS, Lee WJ, Yun TJ, Kim TM, Lee SH, Kim JH, Sohn CH, Park SH, Kim IH, Jahng GH and Chang KH: True progression versus pseudoprogression in the treatment of glioblastomas: A comparison study of normalized cerebral blood volume and apparent diffusion coefficient by histogram analysis. Korean J Radiol *14(4)*: 662-672, 2013.

14 Koh DM and Collins DJ: Diffusion-weighted MRI in the body: applications and challenges in oncology. Am J Roentgenol *188(6)*: 1622-1635, 2007.

15 Steens SC, Admiraal-Behloul F, Schaap JA, Hoogenraad FG, Wheeler-Kingshott CA, le Cessie S, Tofts PS and van Buchem MA: Reproducibility of brain ADC histograms. Eur Radiol *14(3)*: 425-430, 2004.

16 Alvarez E, Westmore M, Galvin RJ, Clapp CL, Considine EL, Smith SJ, Keyes K, Iversen PW, Delafuente DM, Sulaimon S, Zambrano C, Ma L, Sato M, Martin TJ, Teicher BA and Galbreath EJ: Properties of bisphosphonates in the 13762 rat mammary carcinoma model of tumor-induced bone resorption. Clin Cancer Res *9(15)*: 5705-5713, 2003.

17 Joo I, Lee JM, Yoon JH, Jang JJ, Han JK and Choi BI: Nonalcoholic fatty liver disease: Intravoxel incoherent motion diffusion-weighted MR imaging–an experimental study in a rabbit model. Radiology *270(1)*: 131-140, 2014.

18 Le Bihan D, Breton E, Lallemand D, Grenier P, Cabanis E and Laval-Jeantet M: MR imaging of intravoxel incoherent motions: Application to diffusion and perfusion in neurologic disorders. Radiology *161(2)*: 401-407, 1986.

19 Baek HJ, Kim HS, Kim N, Choi YJ and Kim YJ: Percent change of perfusion skewness and kurtosis: A potential imaging biomarker for early treatment response in patients with newly diagnosed glioblastomas. Radiology *264(3)*: 834-843, 2012.

20 Ganeshan B, Miles KA, Young R and Chatwin C: Hepatic entropy and uniformity: Additional parameters that can potentially increase the effectiveness of contrast enhancement during abdominal CT. Clin Radiol *62(8)*: 761-768, 2007.

21 Sharma N, Ray AK, Sharma S, Shukla K, Aggarwal L and Pradhan S: Segmentation of medical images using simulated annealing based fuzzy C means algorithm. Int J Biomed Eng Technol *2(3)*: 260-278, 2009.

22 Albregtsen F: Statistical texture measures computed from gray level coocurrence matrices. Technical Note, Image Processing Laboratory, Department of Informatics, University of Oslo, Norway, 1995.

23 Lee J, Koh D and Ong CN: Statistical evaluation of agreement between two methods for measuring a quantitative variable. Comput Biol Med *19(1)*: 61-70, 1989.

24 Padhani AR, Liu G, Koh DM, Chenevert TL, Thoeny HC, Takahara T, Dzik-Jurasz A, Ross BD, Van Cauteren M, Collins D, Hammoud DA, Rustin GJ, Taouli B and Choyke PL: Diffusion-weighted magnetic resonance imaging as a cancer biomarker: consensus and recommendations. Neoplasia *11(2)*: 102-125, 2009.

25 Jensen LR, Garzon B, Heldahl MG, Bathen TF, Lundgren S and Gribbestad IS: Diffusion-weighted and dynamic contrast-enhanced MRI in evaluation of early treatment effects during neoadjuvant chemotherapy in breast cancer patients. J Magn Reson Imaging *34(5)*: 1099-1109, 2011.

26 Lambregts DM, Beets GL, Maas M, Curvo-Semedo L, Kessels AG, Thywissen T and Beets-Tan RG: Tumour ADC measurements in rectal cancer: Effect of ROI methods on ADC values and interobserver variability. Eur Radiol *21(12)*: 2567-2574, 2011.

27 Koh DM, Blackledge M, Collins DJ, Padhani AR, Wallace T, Wilton B, Taylor NJ, Stirling JJ, Sinha R, Walicke P, Leach MO, Judson I and Nathan P: Reproducibility and changes in the apparent diffusion coefficients of solid tumours treated with combretastatin A4 phosphate and bevacizumab in a two-centre phase I clinical trial. Eur Radiol *19(11)*: 2728-2738, 2009.

28 Goh V, Ganeshan B, Nathan P, Juttla JK, Vinayan A and Miles KA: Assessment of response to tyrosine kinase inhibitors in metastatic renal cell cancer: CT texture as a predictive biomarker. Radiology *261(1)*: 165-171, 2011.

29 Haralick RM: Statistical and structural approaches to texture. Proc IEEE *67(5)*: 786-804, 1979.

30 Kobus T, Vos PC, Hambrock T, De Rooij M, Hulsbergen-Van de Kaa CA, Barentsz JO, Heerschap A and Scheenen TW: Prostate cancer aggressiveness: *in vivo* assessment of MR spectroscopy and diffusion-weighted imaging at 3 T. Radiology *265(2)*: 457-467, 2012.

31 Kyriazi S, Collins DJ, Messiou C, Pennert K, Davidson RL, Giles SL, Kaye SB and Desouza NM: Metastatic ovarian and primary peritoneal cancer: Assessing chemotherapy response with diffusion-weighted MR imaging–value of histogram analysis of apparent diffusion coefficients. Radiology *261(1)*: 182-192, 2011.

32 Tozer DJ, Jager HR, Danchaivijitr N, Benton CE, Tofts PS, Rees JH and Waldman AD: Apparent diffusion coefficient histograms may predict low-grade glioma subtype. NMR Biomed *20(1)*: 49-57, 2007.

33 Koh DM, Collins DJ and Orton MR: Intravoxel incoherent motion in body diffusion-weighted MRI: Reality and challenges. Am J Roentgenol *196(6)*: 1351-1361, 2011.

34 Andreou A, Koh DM, Collins DJ, Blackledge M, Wallace T, Leach MO and Orton MR: Measurement reproducibility of perfusion fraction and pseudodiffusion coefficient derived by intravoxel incoherent motion diffusion-weighted MR imaging in normal liver and metastases. Eur Radiol *23(2)*: 428-434, 2013.

35 Koh DM, Scurr E, Collins DJ, Pirgon A, Kanber B, Karanjia N, Brown G, Leach MO and Husband JE: Colorectal hepatic metastases: Quantitative measurements using single-shot echo-planar diffusion-weighted MR imaging. Eur Radiol *16(9)*: 1898-1905, 2006.

36 Shinmoto H, Oshio K, Tanimoto A, Higuchi N, Okuda S, Kuribayashi S and Mulkern RV: Biexponential apparent diffusion coefficients in prostate cancer. Magn Reson Imaging *27(3)*: 355-359, 2009.

37 Lemke A, Laun FB, Klauss M, Re TJ, Simon D, Delorme S, Schad LR and Stieltjes B: Differentiation of pancreas carcinoma from healthy pancreatic tissue using multiple b-values: Comparison of apparent diffusion coefficient and intravoxel incoherent motion derived parameters. Invest Radiol *44(12)*: 769-775, 2009.

Received February 23, 2014
Revised March 11, 2014
Accepted March 12, 2014